Monte-Carlo-Based Channel Characterization for Underwater Optical Communication Systems

Chadi GABRIEL[1,2], Ali KHALIGHI[1], Salah BOURENNANE[1], Pierre LÉON[2], Vincent RIGAUD[2]

[1] Institut Fresnel, UMR CNRS 7249, Aix-Marseille Université, École Centrale Marseille, Marseille, France

[2] IFREMER, La Seyne Sur Mer, France

Chadi.Gabriel@ifremer.fr, {Ali.Khalighi, Salah.Bourennane}@fresnel.fr, {Pierre.Leon, Vincent.Rigaud}@ifremer.fr

Abstract

We consider channel characterization for underwater wireless optical communication (UWOC) systems. We focus on the channel impulse response and, in particular, quantify the channel time dispersion for different water types, link distances, and transmitter/receiver characteristics, taking into account realistic parameters. We use the Monte Carlo approach to simulate the trajectories of emitted photons propagating in water from the transmitter towards the receiver. During their propagation, photons are absorbed or scattered as a result of their interaction with different particles present in water. To model angle scattering, we use the two-term Henyey-Greenstein model in our channel simulator. We show that this model is more accurate than the usually-used Henyey-Greenstein model, especially in pure sea waters. Through the numerical results that we present, we show that except for highly turbid waters, the channel time dispersion can be neglected when working over moderate distances. In other words, under such conditions, we do not suffer from any inter-symbol interference in the received signal. Lastly, we study the performance of a typical UWOC system in terms of bit-error-rate using the simple on-off-keying modulation. The presented results give insight into the design of UWOC systems.

I. Introduction

Even though oceans and seas cover the majority of the earth surface, they are still generally unexplored. This is especially the case for the deep sea waters. The European FP7 SENSEnet project aims at developing novel sensors for underwater environment monitoring, as well as designing adequate infrastructures for the implementation and deployment of such sensors [1]. Of special interest are the underwater wireless sensor networks (UWSN) due to their flexibility and simplicity of deployment, compared to cabled networks.

An UWSN consists of spatially distributed autonomous nodes to which a number of sensors are connected. These nodes are linked together to exchange the data collected by the sensors. The network can be used for assessing the aqueous environment, monitoring the seafloor activity for disaster prevention (for example, surveillance of seismic activities in order to provide tsunami warnings), helping underwater geochemical prospecting, modeling the weather impact on the submarine life, etc.

Concerning the communication link, special attention should be devoted to the underwater channel properties. Due to their strong attenuation in water, radio frequencies cannot be used, unless over ranges of a few centimeters [2]. Acoustic waves are traditionally used for establishing relatively long range wireless underwater links. However, they are limited in bandwidth and their celerity is very low (around 1500 m/s) leading to serious problems for real-time high-rate communication. Moreover, time synchronization is very difficult, external noise sources considerably affect acoustic signals, and the usually-used large antennas are highly energy consuming [3], [4], [5]. All these make the implementation of an acoustic underwater system problematic in our application.

Optical underwater communication turns to be an appropriate solution for communication over ranges up to several tens of meters thanks to its cost-effectiveness and low-energy consumption [6], [7], [8], [9]. Using a suitable wavelength (in the blue/green range), we can attain high data-rates (up to 1 Gbps over a few meters as reported in [6]), depending on the water conditions and the transmitter/receiver parameters. This can allow data, image, and even video transmission between the nodes of an UWSN. However, optical communication in water is not an easy task since the optical beam is subject to strong intensity attenuation due to light absorption and scattering. In addition, scattering can create inter-symbol interference (ISI) by causing pulse stretching when transmitting with high data rates and over long distances [6], [10]. The induced ISI can degrade the quality of data transmission, and may necessitate computationally complex signal processing (i.e., channel equalization) at the receiver. So, an important step in the design of an UWSN is to accurately characterize the underwater optical channel by taking into account these phenomena. Based on an accurate channel model, one can set the system parameters appropriately in order to establish a high-quality link between the network nodes.

In this work, we consider comprehensive modeling of the underwater optical communication channel based on the Monte Carlo simulation method by which we simulate the trajectories of the emitted photons. We take into account different system parameters such as the transmitter beam width and beam divergence, beam wavelength, water type and turbidity, link distance, and the receiver's field-of-view and aperture size. In particular, we use the two-term Henyey-Greenstein (HG) model for photon scattering which is a more accurate model than the simple Henyey-Greenstein one, considered in [11], [12]. We evaluate the impulse response of the optical channel under different conditions and show that, in most practical cases, the channel time dispersion can effectively be neglected. Also, for demonstration purposes, we consider a typical UWOC system and study its performance in terms of bit-error-rate (BER). For this, we consider the simple on-off-keying (OOK) modulation without channel coding, and illustrate how the BER performance is affected by the link distance and the water type.

The remainder of the paper is organized as follows. In Section II, we briefly present some previous works related to underwater optical propagation modeling while specifying our contributions with respect to them. In Section III, we recall the main characteristics of the water channel and the main equation governing light propagation in water. The description of our Monte Carlo simulator is provided in Section IV and modeling of photon scattering is discussed in Section V. In Section VI, we present some numerical results to identify the channel impulse response (CIR) and to show the impact of different system parameters on the channel time dispersion. Also, we present in this section the BER performance for a simple case study. Finally, Section VII concludes the paper.

II. Previous works related to underwater optical communication

Several recent works have considered channel effects in underwater wireless optical communication. Most of them neglect the channel dispersion due to scattering and use the simple exponential intensity attenuation model for optical beam propagation. In [7], [13], the performance of a wireless underwater optical communication in various water types and at different ranges is studied. In [9], the author considers, in particular, a modulating retro-reflector and a reflective link and shows that using the scattered light can improve the system performance in some special cases. In [2], the authors study the spatial and angular effects of scattering on a laser link based on the radiative transfer equation (RTE) and also present some laboratory experiments.

Two works that have particularly focused on channel time dispersion are those of [10] and [6]. In [10], the author uses the RTE with the modified Stokes vector to model light scattering in water. Considering polarized light, he studies the effect of the transmission distance on the channel time dispersion and concludes that ISI is very restrictive over long ranges (50 m) and at high rates (1 Gbps). However, the water parameters considered in [10] are far from most practical cases and correspond to a too dispersive medium: the average cosine of the scattering angle (see Section V) is set to 0.1348 and the ratio b/c to 0.9767 (see Section III for the definitions of b and c). The difference of our study with [10] is that, here, we take practical system parameters into account, particularly concerning the transmitter and the receiver, and also consider realistic water parameters. Also, we do not take into account light polarization because we consider intensity modulation with non-coherent detection, which is usually used in most systems due to its simplicity.

On the other hand, in [6], the authors present a laboratory experiment for a 1 Gbps-rate optical transmission system over a 2 m path length. They also present the channel transfer function by means of Monte Carlo simulations for longer transmission ranges and for different water types. Here, we consider the CIR as the main channel characteristic instead of the channel transfer function which is considered in [6] and is in fact the Fourier transform of the CIR. We quantify the channel time dispersion, especially for different link distances, transmitter beam divergences, and receiver lens aperture sizes. Furthermore, we study the two-term Henyey-Greenstein (TTHG) model for simulating the trajectories of the scattered photons. Note that while this method is not as precise as the Petzold's experimental measurements [14], it is more accurate than the usually-used HG model and can easily be implemented in the Monte Carlo simulator (see Subsection V-B).

Several laboratory testbeds have also been developed for point-to-point or broadcast underwater optical communication. We provide here a brief presentation of some of them. An underwater sensor network called AquaNodes has been presented in [15], [16]. In this system, in order to reduce energy consumption and system cost, it is proposed to use acoustic links for broadcast communication over ranges up to 400 m (with a typical rate of 300 bps), and optical links for point-to-point communication between nodes over a range of 2 m (with a typical rate of 330 Kbps). Also, a system developed by WHOI has been introduced in [17] as a low-power, low-cost communication system, which uses a set of 22 red LEDs and supports transmission over a range of 5 m with a data-rate of up to 14.4 Kbps. Another prototype is presented in [18] which uses 2 W green/blue LEDs and allows directional transmission over a range of up to 5 m with a data rate of 57.6 Kbps. The AquaOptical system presented in [19] proposes, in particular, a high-rate system for medium range transmission. However, the developed system is highly power consuming: it uses six 5 W LEDs for a data rate of 1 Mbps over 25 m. More recently, a low-cost optical UWSN has been presented in [20] that can work over moderate distances (typically 10 m) but has a very low transmission rate (about 310 bps).

These already-developed systems are not really adequate for our application where we require a node separation on the order of tens of meters and a high transmission rate of more than 10 Mbps. The characterization of the underwater optical channel, that we consider in this paper, is hence an important step in the development of our UWOC system.

III. Characteristics of the optical propagation channel

A. *Effect of water on optical propagation*

The two main processes affecting light propagation in water are absorption and scattering, which are both wavelength dependent [5], [21], [22]. Absorption is the irreversible loss of intensity and depends on the water's index of refraction. The spectral absorption coefficient $a(\lambda)$, with λ being the light wavelength, is the main intrinsic optical property (IOP) to model the water absorption. Scattering, on the other hand, refers to the deflection of light from its original path. In water, deflections can be caused by the particles of size comparable to the wavelength (diffraction), or by the particulate matters with refraction index different from that of the water (refraction). Figure 1 illustrates the propagation behavior of a light flux when encountering a particle. The spectral volume scattering function (VSF) $\beta(\Psi, \lambda)$ is defined as the fraction of incident power scattered out of the beam through an angle Ψ around a solid angle $\Delta\Omega$ centered on $\overline{\Psi}$. The VSF is used as the main IOP to model scattering. Integrating the VSF over all directions, gives the spectral scattering coefficient $b(\lambda)$:

$$b(\lambda) = 2\pi \int_0^\pi \beta(\Psi, \lambda) \sin\Psi \, d\Psi. \tag{1}$$

Another useful parameter is the back-scattering coefficient $b_b(\lambda)$ that is obtained by integrating the VSF in the range $[\pi/2, \pi]$:

$$b_b(\lambda) = 2\pi \int_{\pi/2}^\pi \beta(\Psi, \lambda) \sin\Psi \, d\Psi. \tag{2}$$

Lastly, the spectral beam attenuation coefficient c (also called the extinction coefficient) is defined as the sum of a and b:

$$c(\lambda) = a(\lambda) + b(\lambda). \tag{3}$$

Note that a, b, b_b, and c are in units of m^{-1}.

The performance of an UWOC system can also be affected by channel fading as a result of oceanic turbulence. This is similar to the atmospheric turbulence in free-space optical communication [23], [24]. Water turbulence is generally due to the variations of the water refractive index, caused by the changes in the temperature, salinity, and the pressure of the water [25]. In general, the effect of the pressure on the water refractive index can be neglected [25]. Also, deep seas have generally an approximately constant level of salinity and the temperature variations are usually very small. As a result, the channel fading due to water turbulence can be neglected in most practical cases, as shown in [26].
Lastly, we assume that in our application, i.e., in deep sea, there is no probable beam blockage caused by bubbles, fish, or large suspended particles.

B. Particles in water

In addition to wavelength, both absorption and scattering largely depend on the level of turbidity and the type of particles in solution and suspension in water [27]. The main particles we are concerned with are explained in the following.

- Various dissolved salts which increase the scattering effect.
- Detrital and mineral components such as ground quartz sand, clay minerals, and metal oxides, which affect both absorption and scattering.
- Colored dissolved organic matters (CDOM) such as fluvic and humic acids which affect absorption, especially for blue and ultraviolet wavelengths. Their effect is more pronounced at the water surface and in the estuaries.
- Organic matters such as viruses, colloids, bacteria, phytoplankton, zooplankton, and organic detritus. They contribute in general to backscattering, especially in the blue spectral range.

The spectral absorption and scattering coefficients, a and b, can be calculated by adding the contribution of each class of particles to the corresponding coefficients of the pure sea water. Organic particles and especially phytoplanktonic matters play an important role in the optical properties of most oceanic waters. In fact, their chlorophyll pigments strongly absorb the light in the blue and red spectral ranges. These particles effectively determine the absorbance of the sea water and strongly contribute to the scattering coefficient [12], [28], [29]. Therefore, one can use the chlorophyll concentration C (in mg.m^{-3}) as the free parameter to compute a and b based on the bio-optical model provided in [28], [29] or that proposed by Gordon and Morel [12], for instance.

Let us explicitly see the impact of C on the absorption and scattering properties of water. We have shown in Fig. 2 curves of a, b, and c, as a function of λ using the model in [28], [29] for two chlorophyll concentrations of 0.31 and 0.83 mg.m^{-3}. We notice that an increase in C has a negligible impact on a but it considerably affects b.

C. Water types

Knowing that underwater matters and the water quality are variant from one region to another, four major water types are usually considered in the literature [2], [6], [30]:

- Pure sea waters: Absorption is the main limiting factor. The low b makes the beam propagate approximately in a straight line.
- Clear ocean waters: They have a higher concentration of dissolved particles that affect scattering.
- Coastal ocean waters: They have a much higher concentration of planktonic matters, detritus, and mineral components that affect absorption and scattering.
- Turbid harbor and estuary waters: They have a very high concentration of dissolved and in-suspension matters.

We have indicated in Table I typical values for the parameters a, b, b_b, and c, associated with these water types that we will consider hereafter. For this, we have set the chlorophyll concentration C so as to obtain close values to the attenuation coefficient c provided in [2], [14]. The parameters were calculated using the bio-optical model in [28], [29].

D. Light propagation in water

The behavior of the light radiance in a propagation medium is described by the radiative transfer equation (RTE), given the medium IOP properties and the light beam characteristics. Let us denote by $L(z, \theta, \phi, \lambda)$ the light radiance in units of $\mathrm{Wm^{-2}sr^{-1}nm^{-1}}$, with z being the distance from the transmitter, and θ and ϕ the polar and azimuthal angles, respectively. Let us define the parameter r as $r = z/\cos\theta$. We have [27], [31]:

$$\frac{dL}{d\,r} = -c\,L + L^{\mathrm{E}} + L^{\mathrm{I}} \qquad (\mathrm{Wm^{-3}sr^{-1}nm^{-1}}), \tag{4}$$

where L^{E} and L^{I} denote path functions for elastic and inelastic scattering, respectively. Inelastic scattering corresponds to the loss of photons due to a wavelength change. Because of its relatively low contribution to the general solution of the RTE, we neglect inelastic scattering. Note that most previous works neglect the L^E term, (i.e., scattering) and consider straight-line propagation, described by the simple Lambert's law:

$$L(z) = L(0)\exp(-c\,z). \tag{5}$$

In this paper, we do take scattering into account but instead of solving (4) analytically, we use the Monte Carlo method as described in Sections IV and V.

IV. Channel modeling based on Monte Carlo simulation

We use Monte Carlo simulations based on the MCML method [32] to solve the RTE. Albeit its simplicity and flexibility, it is a rigorous approach for modeling photon transport in water. The main parameters that we take into consideration in our Monte Carlo simulator are:

- The transmitter characteristics, i.e., the wavelength λ, the beam width w_0, and the maximum initial divergence angle denoted here by $\theta_{0,\max}$.
- The distance Z between the transmitter and the receiver, and the medium described by the chlorophyll concentration C.
- The receiver characteristics, i.e., the aperture size and the field-of-view (FOV).

The simulator relies on the local probabilistic rules of photon propagation in water as explained in the following.

A. Initialization

Initially, each photon is launched into the medium with unity weight. Given the beam width w_0 and the maximum initial divergence angle $\theta_{0,\max}$, the initial position and the departure direction of the photon are determined based on three random variables (RVs). The position is generated according to $\mathcal{U}[0, w_0]$, and the direction according to $\mathcal{U}[-\theta_{0,\max}, \theta_{0,\max}]$ for θ and $\mathcal{U}[0, 2\pi]$ for ϕ. Note that $\mathcal{U}[n, m]$ denotes the Uniform distribution between n and m.

B. Interaction of photon with a particle

The considered emitted photon travels a distance δ (what we will refer to as the *step size*) before interacting with a particle in the medium. To generate δ randomly, we use a RV χ_δ of distribution $\mathcal{U}[0, 1]$, and calculate δ using (5) as follows [32].

$$\delta = -\log(\chi_\delta)/c \tag{6}$$

When interacting with the particle, the photon loses a fraction of its initial weight (what we will refer to as *weight drop*) and is deviated from its initial direction (photon scattering). Let us denote the photon weight before and after the interaction by W_{pre} and W_{post}, respectively. We have [27]:

$$W_{\text{post}} = W_{\text{pre}}(1 - a/c). \tag{7}$$

Photon scattering is described in detail in Section V, where we explain how we determine the new propagation direction of the photon (i.e., the new θ and ϕ) after the interaction with a particle.

C. Received photons

This cycle of “step size $\rightarrow$ weight drop $\rightarrow$ angle scattering” is repeated until one of the following events happens:

- The photon weight is too small and negligible. The photon is considered as absorbed. This “photon survival” threshold is set to 10^{-4} by default.
- The photon reaches the receiver plane. If it is in the receiver aperture and FOV, it is considered as effectively received. Otherwise, it is considered as lost.

Our simulator returns the proportion of absorbed, lost, and received photons' weights, as well as the Cartesian coordinates of the point of impact at the receiver and the position of the received photons on the focal plane. In addition, it calculates the total distance traveled by each photon until it reaches the receiver. This parameter can be converted to the propagation delay from the transmitter to the receiver considering a constant speed of light in water ($\approx 2.26 \times 10^8$ m/s).

Considering a photon survival threshold permits to avoid useless too long simulations. This threshold should be decreased for a more-attenuating medium such as turbid waters. For the three other water types, we verified that a threshold of 10^{-4} is sufficient for the results to be presented.

Note that this method is statistical in nature and relies on calculating the propagation of a large number of photons. In our simulations, we have generated at least 10^6 photons for each experiment, and have repeated the experiments at least 10^3 times to obtain reliable results.

V. Photon angle scattering

We explain here how we have modeled photon scattering in our Monte Carlo simulator. As seen in the previous section, after interaction with a particle, the photon is deviated from its incoming direction. The new propagation direction is determined by regenerating randomly the azimuthal angle ϕ and the scattering angle θ. Angle ϕ is considered as a RV of distribution $\mathcal{U}[0, 2\pi]$. The distribution of the scattering angle θ, on the other hand, should take into account the medium characteristics. There are mainly two methods that are considered for modeling the distribution of θ: the simple HG and the TTHG models.

A. Henyey-Greenstein model

Originally proposed for galactic scattering in Astrophysics by Henyey and Greenstein [33], the HG phase function defined by (8) is used in oceanic optics to model light scattering [12].

$$p_{\text{HG}}(\theta, g) = \frac{1 - g^2}{2\,(1 + g^2 - 2g\cos\theta)^{3/2}}. \tag{8}$$

Here, g is the HG asymmetry parameter that depends on the medium characteristics and is equal to the average cosine of the scattering angle θ over all scattering directions, denoted by $\overline{\cos\theta}$. In other words, for the HG model, we take $g = \overline{\cos\theta}$. In fact, (8) describes the probability distribution of the deflection angle θ. It is proposed in [27] to set $g = 0.924$ as a good approximation for most practical situations. In fact, based on the Petzold's measurements of VSF [14], g is calculated in [34] for clean ocean, coastal, and turbid harbor waters. For these three water types, g is equal to 0.8708, 0.9470, and 0.9199, respectively. We have verified that the small difference between these g values has a negligible effect on the optical channel characteristics, especially on the channel time dispersion. This is because the HG model is not accurate at small θ as its shape is broader than most real phase functions (see the next subsection). Another reason is that here we are considering a divergent beam. For collimated beams, the phase function does affect the channel characteristics, as shown in [35]. As a result, we take the average value of $g = 0.924$ proposed in [12] for all water types.

To randomly generate θ, we first generate a RV χ_{HG} of distribution $\mathcal{U}[0, \pi]$, and then calculate the corresponding θ using the following equation.

$$\chi_{\text{HG}} = \int_0^{\theta} p_{\text{HG}}(\Psi, g)\, \sin\Psi\, d\Psi \tag{9}$$

B. Two term Henyey-Greenstein model

The interest of the HG function is its simplicity since it allows an easy computation of the RTE. However, it inadequately describes light scattering in water for small and large angles, namely for $\theta < 20^\circ$ and $\theta > 130^\circ$ [27]. A modified phase function, called the two-term Henyey-Greenstein, has later been proposed in the literature [12], [37], that matches better the experimental results, e.g. those obtained by Petzold [14]. The TTHG function is given by:

$$p_{\text{TTHG}}(\theta, \alpha, g_{\text{FWD}}, g_{\text{BKWD}}) = \alpha\, p_{\text{HG}}(\theta, g_{\text{FWD}}) + (1-\alpha)\, p_{\text{HG}}(\theta, -g_{\text{BKWD}}), \tag{10}$$

where α is the weight of the forward-directed HG phase function, and g_{FWD} and g_{BKWD} are the asymmetry factors for forward- and backward-directed HG phase functions, respectively. Relationships between g_{FWD}, g_{BKWD}, α, and $\overline{\cos\theta}$, are provided in [37], [38] and reproduced in the following.

$$g_{\text{BKWD}} = -0.3061446 + 1.000568\, g_{\text{FWD}} - 0.01826338\, g_{\text{FWD}}^2 + 0.03643748\, g_{\text{FWD}}^3 \tag{11}$$

$$\alpha = \frac{g_{\text{BKWD}}(1+g_{\text{BKWD}})}{(g_{\text{FWD}}+g_{\text{BKWD}})(1+g_{\text{BKWD}}-g_{\text{FWD}})} \tag{12}$$

$$\overline{\cos\theta} = \alpha(g_{\text{FWD}}+g_{\text{BKWD}}) - g_{\text{BKWD}} \tag{13}$$

In addition, an approximate equation, obtained via regression on the experimental data of [39], is proposed in [38]:

$$\overline{\cos\theta} = 2\,\frac{1-2B}{2+B}, \tag{14}$$

where $B = b_b/b$. Now, given b and b_b, using (11)-(14) we calculate the parameters $\overline{\cos\theta}$, g_{FWD}, g_{BKWD}, and α. Then, we generate a RV χ_{TTHG} of distribution $\mathcal{U}[0,\pi]$ and use it to calculate the corresponding θ similar to (9).

We have compared in Fig. 3 the phase functions based on the HG and TTHG photon scattering models with the experimental measurements of Petzold [14]. Unfortunately, we could not find in Petzold's tables the data for $\overline{\cos\theta} = 0.924$ that we consider in this paper. Instead, we have compared the phase functions for $B = 0.038$ corresponding to a close average cosine value, $\overline{\cos\theta} = 0.907$. We notice that the TTHG model predicts better the Petzold's phase function points, especially at small angles where the phase function has its largest values. The HG model predicts a broader shape for the phase function. A similar comparison for $B = 0.119$ (corresponding to $\overline{\cos\theta} = 0.719$) can be found in [37].

VI. Numerical results

We provide here some simulation results mainly to study the characteristics of the underwater optical channel. We consider a line-of-sight configuration where the transmitter and the receiver are perfectly aligned. At the receiver, we use a lens of diameter D and a high speed photo-detector (PD) placed on its focal point. We consider the following typical parameters in our system by default: the wavelength $\lambda = 532\,\text{nm}$, a beam width of $w_0 = 3\,\text{mm}$, a maximum beam divergence of $\theta_{0,\max} = 20°$, a link distance of $Z = 20\,\text{m}$, and a receiver lens diameter of $D = 20\,\text{cm}$. Furthermore, we work by default in clear ocean waters with the typical C of 0.31 mg.m^{-3}. We do not consider any spatial filtering at the receiver because in deep-sea waters, in which we are particularly interested, we can effectively neglect background radiations. For the general results to be presented in the following, we intentionally do not limit the receiver FOV in order to see the worst impact concerning the channel time dispersion due to the scattered photons. In other words, unless otherwise mentioned, we take into account all the photons arriving on the receiver lens, which is equivalent to take FOV$= 180°$. We will study the impact of the main system parameters on the underlying optical channel, and in particular, on the CIR.

A. Received intensity as a function of distance

Let us start by considering the effect of the attenuation coefficient c on the total received intensity that we denote by I_r. We have shown in Fig. 4 curves of I_r as a function of distance Z for the four water types specified in Table I. (Note that the values in dB correspond to $10\log_{10} I_r$ as the intensity is considered as the optical power.) Results are presented for the HG scattering model with $\overline{\cos\theta} = 0.924$, and the TTHG model while calculating $\overline{\cos\theta}$ from (14). For instance, for the pure sea water case, we have $b = 0.00296\,\mathrm{m}^{-1}$ and $b_b = 0.00085\,\mathrm{m}^{-1}$, resulting in $B = 0.1969$ and $\overline{\cos\theta} = 0.3696$. On the other hand, for the clean ocean waters, for instance, we have $b = 0.08042\,\mathrm{m}^{-1}$ and $b_b = 0.00105\,\mathrm{m}^{-1}$, resulting in $B = 0.0131$ and $\overline{\cos\theta} = 0.967$ [12], [29]. Considering a given water type, we notice a difference between the results corresponding to the two photon scattering models. This difference is mainly due to the better approximation of small and large angle photon scattering in the TTHG model, as discussed in Section V and illustrated in Fig. 3. It is also due to the difference of the $\overline{\cos\theta}$ for the two cases. In fact, in the TTHG model, $\overline{\cos\theta}$ depends on the water type, unlike the HG model where it is set to 0.924. In particular, for the case of pure sea waters, we have a large difference between $\overline{\cos\theta}$ by the HG and TTHG models, that leads to a significant difference between the I_r curves.

Let us now focus on the results corresponding to the TTHG model. Let us assume a tolerable loss of 50 dB beyond which the signal is not detectable at the receiver. Note that, in practice, this limit depends on the transmitter power and the receiver sensitivity. With this assumption, we notice from Fig. 4 that the transmission range is limited to 27 m, 46 m, and 98 m, for coastal, clear ocean, and pure sea waters, respectively. When working in turbid or estuary waters, on the other hand, the high signal attenuation limits the communication range to less than 5 m. Obviously, the range limit depends on the aperture size, because increasing D allows collecting more scattered photons [11].

Afterwards, the simulation results that we present are obtained based on the TTHG model for photon scattering.

B. Channel impulse response

The most useful information concerning the channel is its impulse response using which one can quantify the signal attenuation and the time dispersion. We have conducted four sets of simulations to study the CIR for different cases of water type, receiver's lens diameter, transmitter beam parameters, and link distance. To quantify the time dispersion, usually a parameter called delay spread is considered that is defined as the duration over which the CIR falls below a threshold [40]. Here, we define the delay spread τ, as the duration over which the CIR falls to $-20\,$dB below its peak. Obviously, the larger the delay spread τ, the more is the risk of frequency selectivity. Note that if τ is defined considering less exigent conditions (e.g. a lower threshold of $-10\,$dB), we may still neglect the ISI in practice if τ is negligible compared to the symbol duration. However, in the results to be presented, we will consider the threshold of $-20\,$dB so as to draw indisputable conclusions. The main results concerning the study of the CIR presented below, are summarized in Table II.

1) CIR for different water types: The CIRs for pure sea, clean ocean, and coastal waters are compared in Fig. 5 considering the default values for the other system parameters. The abscissa represents the absolute propagation time from the transmitter to the receiver. For the sake of completeness, we have also indicated the attenuation length which is defined as the product cZ on the figure. The case of turbid harbor waters is not represented because too few photons can reach the distance of $Z = 20\,$m for this water type, as it can be seen from Fig. 4. We notice that the channel dispersion τ is about 0.21 ns, 0.26 ns, and 0.28 ns, for pure sea, clean ocean, and coastal water cases, respectively. So, for typical data-rates (below Gbps), the channel can practically be considered as non-dispersive, and ISI as negligible for these water types.

Let us consider the case of turbid waters separately. We have shown in Fig. 6 the CIR for the case of $Z = 6$ and 8 m with the other default parameters. In order to deal with this highly attenuating and scattering case, we have removed the photon survival threshold in our Monte Carlo simulations. Note that this leads to much longer simulation times. Compared to the previous cases, we have also increased the number of generated photons to more than ten times to obtain the intensity profile at the receiver, because it is very difficult to obtain a smooth CIR due to too few photons that can reach the receiver. For $Z = 6\,\mathrm{m}$, the delay spread τ remains very small and equals 0.6 ns. For $Z = 8\,\mathrm{m}$, however, τ is about 3 ns and the channel is effectively frequency selective. Nevertheless, we note that communication over such distances requires very high power emitters; for instance, the intensity loss is about -82.3 dB at $Z = 8\,\mathrm{m}$. These results are in accordance with the experimental studies in [2], [35], [36] where it is shown that for attenuation lengths cZ larger than 10, the scattering effect becomes important and predominates for $cZ > 15$. As indicated in Fig. 6, for the two considered link distances, we have $cZ = 13.02$ and 17.36. The interesting point in Fig. 6 is that, compared to the previously considered water types, here we have less photons that reach the receiver via the direct path and, consequently, the CIR peak occurs slightly after.

2) Effect of the receiver's lens aperture size: The effect of the receiver's lens diameter D on the CIR is illustrated in Fig. 7 for clean ocean waters. We have intentionally considered the two extreme cases of $D = 0.5$ cm (too small) and 50 cm (too large) to see clearly the impact on the CIR. Obviously, the use of a larger lens allows the collection of more photons: we notice a 22.5 dB increase in the CIR peak by increasing D from 0.5 cm to 50 cm. Enlarging the receiver lens also results in the collection of more scattered photons and hence in widening the CIR. For instance, τ is increased from 0.22 ns to 0.32 ns by increasing D from 0.5 cm to 50 cm. Nevertheless, we notice that, even by using a large lens of $D = 50$ cm, we practically do not suffer from ISI in low turbidity waters.

3) Impact of link distance: Figure 8 shows the channel CIR for $D = 20$ cm and three link distances of $Z = 10$ m, 20 m, and 50 m. Note that in this figure, the CIRs are plotted relative to the respective propagation time for each distance Z in order to see better the details of the curves. As expected, the channel becomes more dispersive by increasing Z. The channel dispersion τ is about 0.24 ns, 0.26 ns, and 0.43 ns for the three Z values, respectively. The interesting result is that τ remains negligible even for a relatively long distance of 50 m.

4) Impact of the transmitter parameters: We have investigated the effect of the transmitter beam width w_0 and the maximum initial beam divergence angle $\theta_{\max}$ on the channel dispersion.

We noticed that w_0 has a negligible impact on τ unless for a too small receiver aperture (results are not shown for the sake of brevity). For instance, for the default case of clear ocean waters and $Z = 20\,\mathrm{m}$, increasing w_0 from 3 mm to 30 cm results in an increase of τ from 0.26 ns to 0.27 ns only, while the peak of the CIR is reduced by 3 dB. On the other hand, the parameter $\theta_{\max}$, affects considerably the CIR peak since it directly influences channel attenuation. In addition, for a larger $\theta_{\max}$, photons are deviated more from the optical axis, leading to a larger τ. The CIR parameters are compared in Table II for $\theta_{\max} = 0,\ 20°$, and $45°$, as well as for $w_0 = 0.3$, 3, and 30 cm.

C. Case study

In this section, we give an insight into an UWSN system design by considering a simple communication system and by evaluating its BER performance versus the link distance. We consider the default system parameters defined in the previous subsection as well as the cases of clean ocean and coastal waters. We assume that the transmitter and the receiver are perfectly aligned and time synchronized. We use the simple OOK modulation without any error correcting coding and set the bit rate to 100 Mbps. At the receiver, after photo-detection, the photo-current is converted to a voltage by a trans-impedance (TZ) circuitry and the resulting signal is low-pass filtered to limit the thermal noise variance [41]. Then, we time sample the signal and proceed to signal detection based on optimum thresholding. In contrary to atmospheric (free-space) optical communication [42], here the background noise can be neglected because our UWSN has to be deployed in deep waters where the sunlight cannot penetrate. We consider a lens of diameter $D = 20\,\mathrm{cm}$ and focal distance of $F = 25\,\mathrm{cm}$. For the PD, we consider an active area of 3.0 mm in diameter (see Subsection VI-C.2 below). The PD is placed at the focal plane of the receiver collecting lens. Also, The TZ resistance is set to 50 Ω.

1) Photon loss due to limited PD active area: Prior to BER calculation, we should first determine the percentage of the photons that can be captured on the PD active area, given the optics of the receiver. For this purpose, we should first calculate the receiver FOV, given the PD size and the receiver lens focal distance. For a given PD active area, we should take into account the limited FOV of the receiver. Notice that, up to now, we had considered a FOV of

180° to study the worst case concerning channel time dispersion. Let us denote the PD active area diameter by D_{aa}. The receiver FOV can be calculated as follows [43].

$$\text{FOV} = 2\,\arctan\left(\frac{D_{\text{aa}}}{2\,F}\right) \tag{15}$$

For $D_{\text{aa}} = 3\,\text{mm}$ and $F = 25\,\text{cm}$, we have FOV $= 0.69^\circ$. To calculate the percentage of photons arriving on the PD active area, we note that for a photon arriving at the receiver lens with an incident angle Θ with respect to the optical axis, the corresponding impact point on the focal plane will be of distance d from the lens focal point, where [43]:

$$d = -F\ \tan(\Theta). \tag{16}$$

Using our Monte Carlo simulator, we have obtained the distribution of the received intensity on the focal plane. The corresponding distributions for $F = 25\,\text{cm}$ are shown in Fig. 9 for the two cases of clear ocean and coastal waters. For demonstration simplicity, we have presented one-dimensional distributions. The form of the intensity distribution around $d = 0$ is due to the TTHG phase function form at small angles (see Fig. 3). Notice that we neglect the photon loss due to reflections at the receiver lens' boundaries [44]. Given $D_{\text{aa}} = 3\,\text{mm}$, we have calculated the percentage of the received photons that are lost due to the limited PD active area. For the cases of clear ocean and coastal waters, we have a loss of 11% and 21% in the received intensity, respectively. This loss is taken into account in BER calculation in the following subsection.

2) Bit-error-rate performance: Let us consider the BER performance as a function of the distance Z. We consider the use of uncoded OOK modulation and the two cases of PIN and avalanche photodiode (APD) photo-detectors. Using the Monte Carlo simulator, we calculate the received intensity on the PD active area. Then, the BER can be calculated for the case of PIN [23]. For the case of APD, we use numerical simulations to calculate the BER.

We firstly consider the case of a Si PIN PD. For this, we use the characteristics of the Si-PIN Hamamatsu S10784 [45]: it has a cut-off frequency of 250 MHz, a sensitivity of $R_\lambda = 0.35$ A/W at $\lambda = 532\,\text{nm}$ corresponding to a quantum efficiency of $\eta = 0.82$ [46], and an active area diameter of 3.0 mm. Note that, for the case of a PIN PD, the dominant noise at the receiver is the thermal noise [41]. Figure 10 shows the BER curves for two cases of $P_t = 0.1$ W and 1 W, where P_t is the transmit (optical) power. If we consider a required BER of 10^{-6}, the maximum distances for reliable data transmission are about $26\,\mathrm{m}$ and $16.5\,\mathrm{m}$ for $P_t = 0.1\,\mathrm{W}$, and about $39\,\mathrm{m}$ and $24\,\mathrm{m}$ for $P_t = 1\,\mathrm{W}$, for the two cases of clear ocean and coastal waters, respectively.

Now, consider the case where an APD is used at the receiver. For this case, we use the characteristics of the Si APD Hamamatsu S8664-30K [45]: it has a bandwidth of 140 MHz, a quantum efficiency of $\eta = 0.78$ at $\lambda = 532\,\mathrm{nm}$, and the same active area diameter 3 mm as the PIN PD considered before. Also, it has a maximum gain of 50. Note that for the case of an APD, shot noise is the dominant noise source at the receiver [41]. Consequently, for each distance Z, we calculate the optimum APD gain that maximizes the receiver SNR [47]. Figure 11 shows the BER curves for $P_t = 0.1\,\mathrm{W}$ and $1\,\mathrm{W}$. We notice that a significant increase in the link distance can be achieved by replacing the PIN PD with an APD. For the target BER of 10^{-6}, the maximum distances for reliable data transmission are about $48\,\mathrm{m}$ and $29\,\mathrm{m}$ for $P_t = 0.1\,\mathrm{W}$, and about $64.5\,\mathrm{m}$ and $37.5\,\mathrm{m}$ for $P_t = 1\,\mathrm{W}$, for the two cases of clear ocean and coastal waters, respectively. However, this advantage becomes at the expense of increased implementation complexity, in particular, concerning the receiver electronics. For the considered S8664-30K APD, we need a voltage of about 350 V for APD reverse biasing.

VII. Conclusions

We presented in this paper a realistic model for underwater wireless optical channels using an elaborate Monte Carlo simulator. When used for an initial system design, our model is more realistic than the simple Lambert law, because the latter leads to a too optimistic predicted system performance by neglecting the scattering effect. It is also more accurate than the previously proposed model based on the simple HG phase function. We took different parameters such as the water type and the characteristics of the transmitter and the receiver into account. Through this study, we confirmed that when the scattering albedo is moderate, the channel delay spread is negligible. In highly turbid waters, however, channel dispersion could affect the data transmission if the communication takes place over relatively large distances. We focused on optical communication in clear ocean waters, which is the object of the particular UWSN that we consider, related to this work. For such conditions, we showed that the channel can effectively be considered as frequency non-selective even when working over distances up to 50 m. Therefore, we practically do not suffer from any ISI and do not need to perform computationally complex signal processing such as channel equalization at the receiver. Finally, we studied the performance of a typical UWOC system in terms of BER using the simple OOK modulation and considering off-the-shelf PIN and APD detectors at the receiver.

This work has been an important phase based on which we can now proceed to the next steps of the UWSN design.

ACKNOWLEDGMENT

This work has been supported in part by SENSEnet, a Marie Curie Initial Training Network (ITN) funded by the European Commission Seventh Framework Programme, Contract Number PITN-GA-2009-237868. The authors wish to thank Dr. Anabela Dasilva from Institut Fresnel, Marseille, France, for the fruitful discussions on the radiative transfer theory and the Monte Carlo simulation method. They are also grateful to Prof. Hassan Akhouayri and Dr. Frédéric Lemarquis from Institut Fresnel, for the discussions on the implementation aspects concerning the transmitter/receiver optics. Parts of this work have been presented in IEEE Workshop on Optical Wireless Communications, Global Communication Conference, 2011 (Reference [11]).

REFERENCES

[1] *International Sensor Development Network*, SENSEnet, http://www.eu-sensenet.net/.

[2] B. M. Cochenour, L. J. Mullen, and A. E. Laux, "Characterization of the beam-spread function for underwater wireless optical communications links," *IEEE Journal of Oceanic Engineering*, vol. 33, no. 4, pp. 513–521, Oct. 2008.

[3] I. F. Akyildiz, D. Pompili, and T. Melodia, "Underwater acoustic sensor networks: research challenges," Ad Hoc Networks, vol. 3, no. 3, pp. 257–279, 2005.

[4] G. Shah, "A survey on medium access control in underwater acoustic sensor networks," in *International Conference Workshops on Advanced Information Networking and Applications (WAINA)*, May 2009, pp. 1178–1183, Bradford, UK.

[5] F. Pignieri, F. De Rango, F. Veltri, and S. Marano, "Markovian approach to model underwater acoustic channel: Techniques comparison," in *Military Communications Conference (MILCOM)*, Nov. 2008, pp. 1–7, San Diego, CA.

[6] F. Hanson and S. Radic, "High bandwidth underwater optical communication," *Applied Optics*, vol. 47, no. 2, pp. 277–283, Jan. 2008.

[7] J. W. Giles and I. Bankman, "Underwater optical communcations systems. Part 2: Basic design considerations," in *IEEE Military Communications Conference (MILCOM)*, Oct. 2005, vol. 3, pp. 1700–1705, Atlantic City, NJ.

[8] D. Anguita, D. Brizzolara, and G. Parodi, "Building an underwater wireless sensor network based on optical communication: research challenges and current results," *International Conference on Sensor Technologies and Applications, SENSORCOMM*, pp. 476–479, Aug. 2009, Athens, Greece.

[9] S. Arnon, "Underwater optical wireless communication network," *Optical Engineering*, vol. 49, no. 1, pp. 1–6, Jan. 2010.

[10] S. Jaruwatanadilok, "Underwater wireless optical communication channel modeling and performance evaluation using vector radiative transfer theory," *IEEE Journal on Selected Areas in Communications*, vol. 26, no. 9, pp. 1620–1627, Dec. 2008.

[11] C. Gabriel, M. A. Khalighi, S. Bourennane, P. Léon, and V. Rigaud, "Channel modeling for underwater optical communication," *IEEE Workshop on Optical Wireless Communications, Global Communication Conference*, pp. 833–837, Dec. 2011, Houston, TX.

[12] C. D. Mobley, *Light and Water: Radiative Transfer in Natural Waters*, Academic Press, June 1994.

[13] J. H. Smart, "Underwater optical communications systems. Part 1: Variability of water optical parameters," in *IEEE Military Communications Conference*, Oct. 2005, vol. 2, pp. 1140–1146, Atlantic City, NJ.

[14] T. J. Petzold, "Volume scattering functions for selected ocean waters," Technical Report SIO 7278, Scripps Institute of Oceanography, 1972.

[15] I. Vasilescu, K. Kotay, D. Rus, M. Dunbabin, and P. Corke, "Data collection, storage, and retrieval with an underwater sensor network," in *International Conference on Embedded Networked Sensor Systems (SenSys)*, Nov. 2005, pp. 154–165, San Diego, CA.

[16] I. Vasilescu, C. Detweiler, and D. Rus, "Aquanodes: An underwater sensor network," in *Workshop on Underwater networks (WuWNet), MobiCom Conference*, Sept. 2007, pp. 85–88, Montreal, Canada.

[17] M. Tivey, P. Fucile, and E. Sichel, "A low power, low cost, underwater optical communication system," *Ridge 2000 Events*, pp. 27–29, Apr. 2004.

[18] F. Schill, U. R. Zimmer, and J. Trumpf, "Visible spectrum optical communication and distance sensing for underwater applications," *Australian Conference on Robotics and Automation (ACRA)*, Dec. 2004, Canberra, Australia.

[19] M. Doniec, I. Vasilescu, M. Chitre, and C. Detweiler, "AquaOptical: A lightweight device for high-rate long-range underwater point-to-point communication," *IEEE OCEANS Conference*, pp. 1–6, Oct. 2009, Biloxi, MS.

[20] J. Lu, S. Lee, J. Mounzer, and C. Schurgers, "Low-cost medium range optical underwater modem," in *ACM International Workshop on UnderWater Networks (WUWNet)*, Nov. 2009, Berkeley, CA.

[21] C.D. Mobley, B. Gentili, H. R. Gordon, Z. Jin, G. W. Kattawar, A. Morel, P. Reinersman, K. Stamnes, and R. H. Stavn, "Comparison of numerical models for computing underwater light fields," *Applied Optics*, vol. 32, no. 36, pp. 7484–7504, Dec. 1993.

[22] D. J. Bogucki, J. Piskozub, M.-E. Carr, and G. D. Spiers, "Monte carlo simulation of propagation of a short light beam through turbulent oceanic flow," *Optics Express*, vol. 15, no. 21, pp. 13988–13996, Oct. 2007.

[23] L. C. Andrews and R. L. Phillips, *Laser Beam Propagation Through Random Media*, SPIE Press, second edition, 2005.

[24] M. A. Khalighi, N. Schwartz, N. Aitamer, and S. Bourennane, "Fading reduction by aperture averaging and spatial diversity in optical wireless systems," *IEEE/OSA Journal of Optical Communications and Networking*, vol. 1, no. 6, pp. 580–593, Nov. 2009.

[25] J. A. Simpson, B. L. Hughes, and J. F. Muth, "A spatial diversity system to measure optical fading in an underwater communications channel," in *IEEE OCEANS Conference*, Oct. 2009, pp. 1–6, Biloxi, MS.

[26] F. Hanson and M. Lasher, "Effects of underwater turbulence on laser beam propagation and coupling into single-mode optical fiber," *Applied Optics*, vol. 49, no. 16, pp. 3224–3230, June 2010.

[27] C. F. Bohren and D. R. Huffman, *Absorption and Scattering of Light by Small Particles*, Wiley, 1988.

[28] V. I. Haltrin and G. W. Kattawar, "Self-consistent solutions to the equation of transfer with elastic and inelastic scattering in oceanic optics: I. Model," *Applied Optics*, vol. 32, no. 27, pp. 5356–5367, 1993.

[29] V. I. Haltrin, "Chlorophyll-based model of seawater optical properties," *Applied Optics*, vol. 38, no. 33, pp. 6826–6832, Nov. 1999.

[30] G. Kervern, "Lidars sous-marins," *Techniques de l'Ingénieur*, vol. 6, no. E4325, pp. 1–7, Nov. 1997.

[31] A. Ishimaru, *Wave Propagation and Scattering in Random Media*, IEEE Press, 1997.

[32] L. Wang, S. L. Jacques, and L. Zheng, "MCML, Monte Carlo modeling of light transport in multi-layered tissues," Tech. Rep., Laser Biology Research Laboratory, Nov. 1995, University of Texas, M.D. Anderson Cancer Center.

[33] H. C. van de Hulst, *Light Scattering by Small Particles*, Dover Publications, 1981.

[34] Yu I. Kopilevich, M. E. Kononenko, and E. I. Zadorozhnaya, "The effect of the forward-scattering index on the characteristics of a light beam in sea water," *Journal of Optical Technology*, vol. 77, no. 10, pp. 598–601, Oct. 2010.

[35] L. Mullen, D. Alley, and B. Cochenour, "Investigation of the effect of scattering agent and scattering albedo on modulated light propagation in water," *Applied Optics*, vol. 50, no. 10, pp. 1396–1404, Apr. 2011.

[36] B. Cochenour and L. Mullen and J. Muth, "Effect of scattering albedo on attenuation and polarization of light underwater," *Optics Letters*, vol. 35, no. 12, pp. 2088-2090, June 2010.

[37] V. Haltrin, "One-parameter two-term henyey-greenstein phase function for ligth scattering in seawater," *Applied Optics*, vol. 41, no. 6, pp. 1022–1028, Feb. 2002.

[38] V. I. Haltrin, "Two-term henyey-greenstein light scattering phase function for seawater," *International Geoscience and Remote Sensing Symposium (IGARSS)*, pp. 1423–1425, June-July 1999, Hamburg, Germany.

[39] V. Timofeyeva, "Relation between light-field parameters and between scattering phase function characteristics of turbid media, including seawater," *Ocean Physics*, vol. 14, pp. 834–848.

[40] J. D. Gibson, Ed., *Mobile Communications Handbook*, CRC Press, Springer, IEEE Press, second edition, 1999.

[41] F. Xu, M. A. Khalighi, and S. Bourennane, "Impact of different noise sources on the performance of PIN- and APD-based FSO receivers," COST IC0802 Workshop, IEEE ConTEL Conference, pp. 279–286, June 2011, Graz, Austria.

[42] M. A. Khalighi, F. Xu, Y. Jaafar, and S. Bourennane, "Double-laser differential signaling for reducing the effect of background radiation in free-space optical systems," *IEEE/OSA Journal of Optical Communications and Networking*, vol. 3, no. 2, pp. 145–154, Feb. 2011.

[43] M. Katz, *Introduction to Geometrical Optics*, World Scientific Pub Co Inc, 2002.

[44] B. E. A. Saleh and M. C. Teich, *Fundamentals of Photonics*, Wiley, 1991.

[45] *Hamamatsu Opto-semiconductor products*, http://jp.hamamatsu.com/products/sensor-ssd/index_en.html.

[46] D. G. Steel and L. Bayvel, Eds., *Encyclopedia of Modern Optics*, vol. 1, Elsevier, 2004.

[47] K. Kiasaleh, "Performance of APD-based, PPM free-space optical communication systems in atmospheric turbulence," *IEEE Transactions on Communications*, vol. 53, no. 9, pp. 1455–1461, Sept. 2005.

TABLE I

ABSORPTION, SCATTERING, BACK SCATTERING, AND ATTENUATION COEFFICIENTS FOR THE FOUR WATER TYPES CONSIDERING TYPICAL CHLOROPHYLL CONCENTRATIONS.

Water type	C (mg/m^3)	a (m^{-1}	b (m^{-1})	b_b (m^{-1})	c (m^{-1})
Pure sea	0.005	0.053	0.003	0.0006	0.056
Clear ocean	0.31	0.069	0.08	0.0010	0.15
Coastal	0.83	0.088	0.216	0.0014	0.305
Turbid harbor	5.9	0.295	1.875	0.0076	2.17

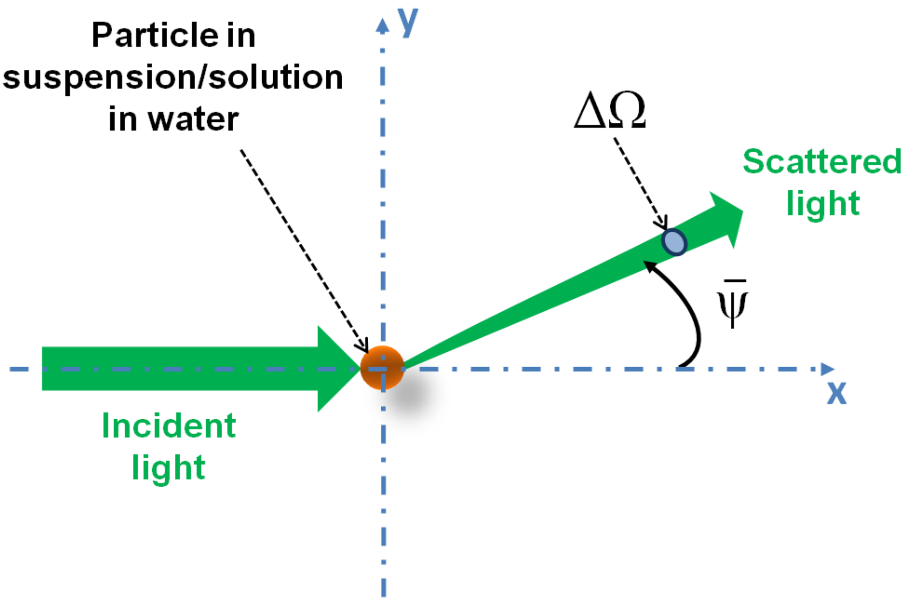

Fig. 1. Light scattering when encountering a particle in water. Part of the incident light flux is absorbed by the particle and the remaining flux is scattered through an angle Ψ. The scattering direction Ψ is within a solid angle $\Delta\Omega$ around $\overline{\Psi}$.

TABLE II

SUMMARY OF INTENSITY LOSS AND CHANNEL TIME DISPERSION FOR DIFFERENT SYSTEM AND CHANNEL PARAMETERS.

(THE DEFAULT CASE APPEARS IN THE FIRST ROW)

c (m^{-1})	Z (m)	D (cm)	$\theta_{\max}$ ($^\circ$)	w_0 (cm)	Intensity loss (dB)	τ (ns)
0.15	**20**	**20**	**20**	**0.3**	$\mathbf{-30.41}$	**0.26**
0.056	20	20	20	0.3	-23.50	0.21
0.305	20	20	20	0.3	-39.74	0.28
2.17	**8**	20	20	0.3	-82.32	≈ 3
0.15	20	**0.5**	20	0.3	-48.38	0.22
0.15	20	**2**	20	0.3	-41.44	0.24
0.15	20	**50**	20	0.3	-25.89	0.32
0.15	**10**	20	20	0.3	-21.23	0.24
0.15	**50**	20	20	0.3	-53.52	0.43
0.15	20	20	20	**3**	-30.44	0.26
0.15	20	20	20	**30**	-33.12	0.28
0.15	20	20	**0**	0.3	-12.28	0.17
0.15	20	20	**45**	0.3	-33.94	0.27

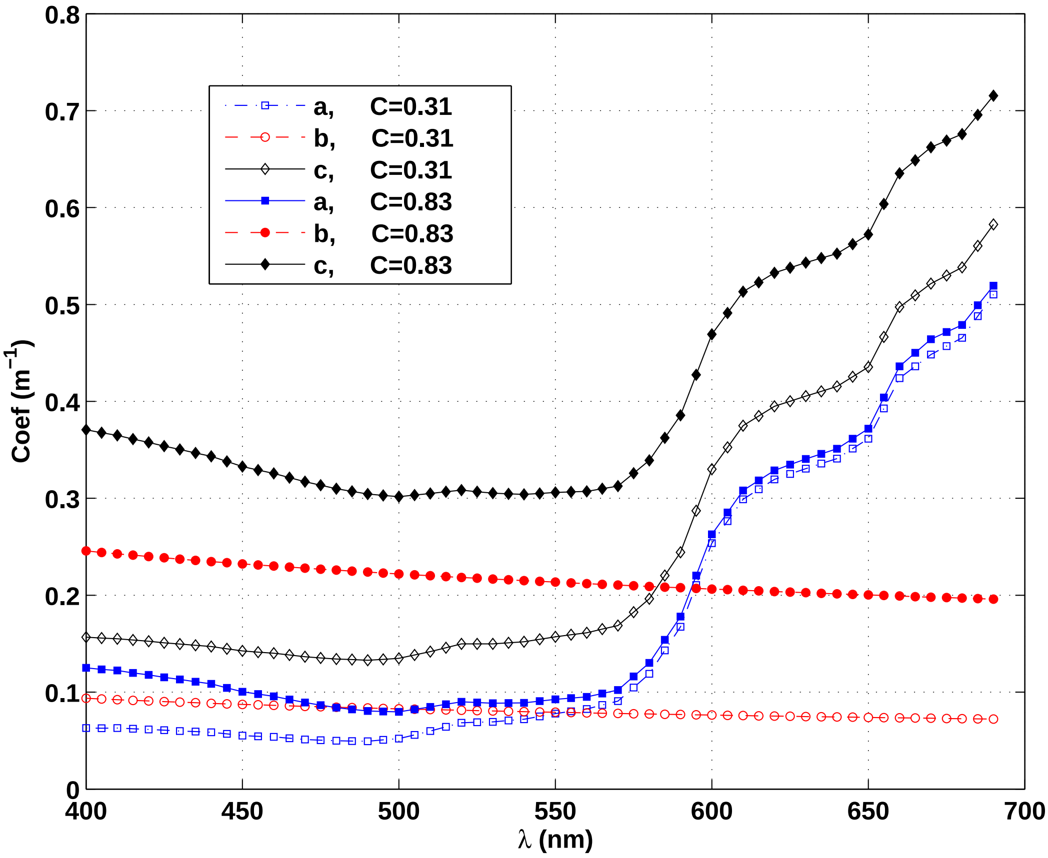

Fig. 2. Absorption a, scattering b, and attenuation c coefficients as a function of the wavelength λ for two chlorophyll concentrations C (in mg.m^{-3}) corresponding to clear ocean and coastal waters, using the model in [28], [29].

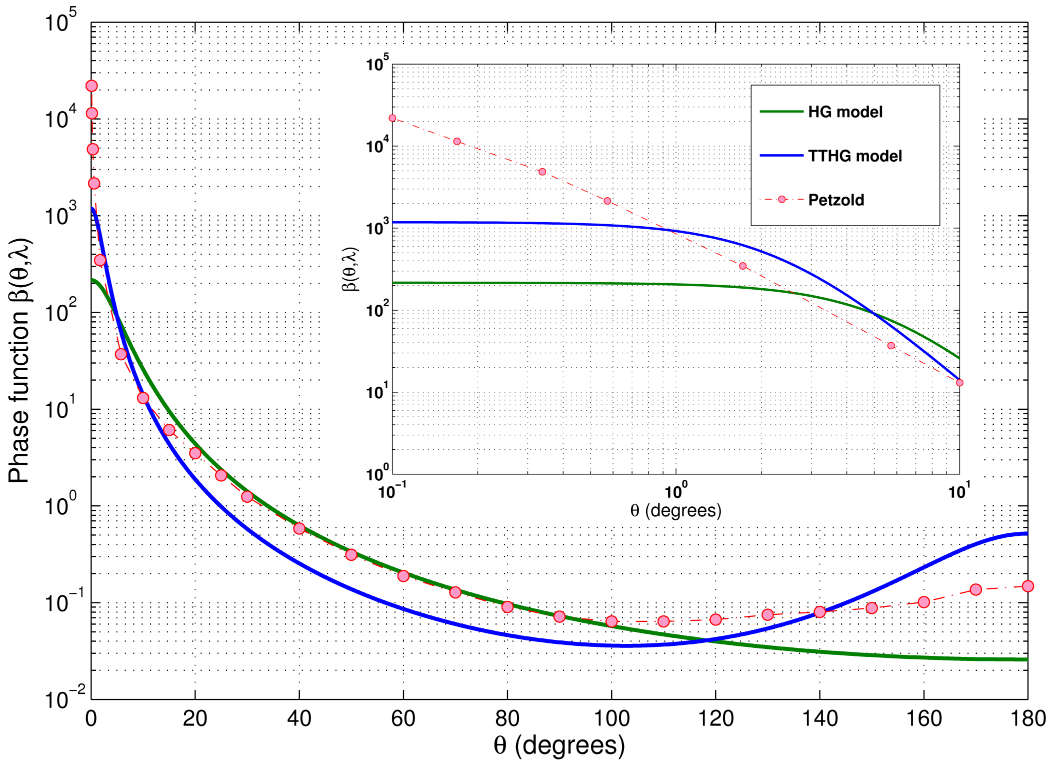

Fig. 3. Contrasting HG and TTHG phase functions with Petzold's experimental measurements [14] for $B = b_b/b = 0.038$. To see better the difference of the phase functions for small angles, the figure is enlarged and displayed in log-scale for $\theta < 10°$.

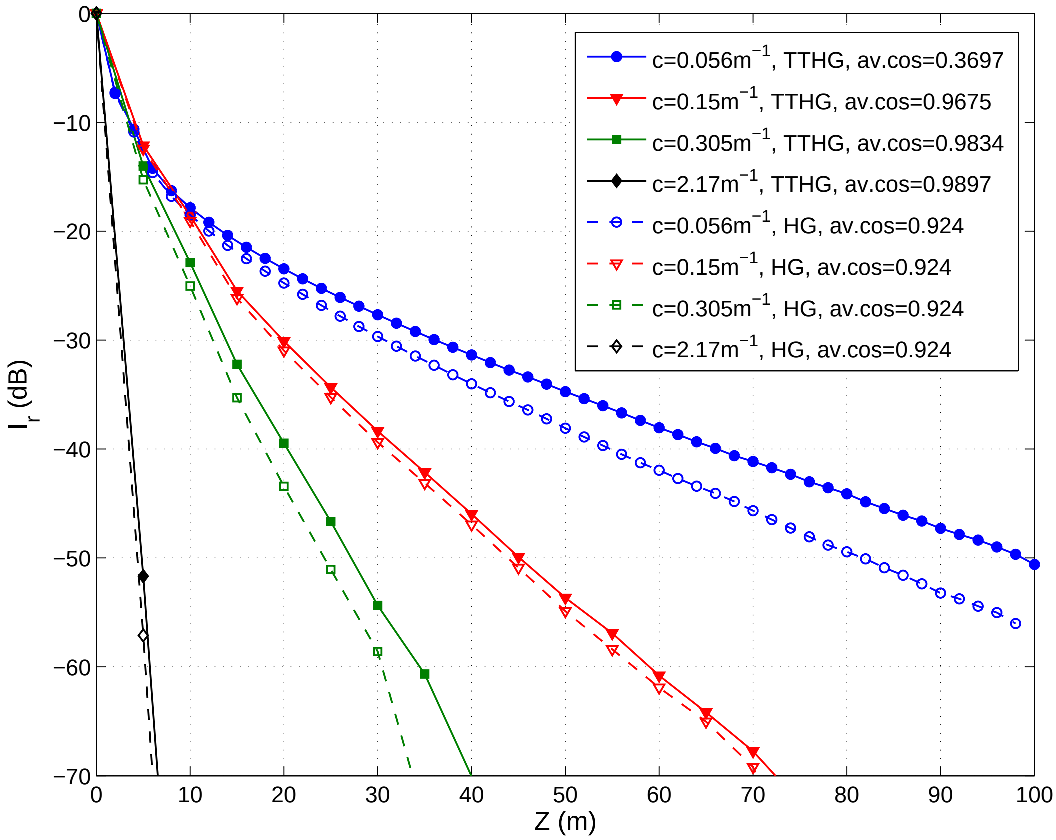

Fig. 4. Received intensity (in dB) as a function of distance for different water types, $D = 20\,\text{cm}$. “av. cos” denotes $\overline{\cos\theta}$.

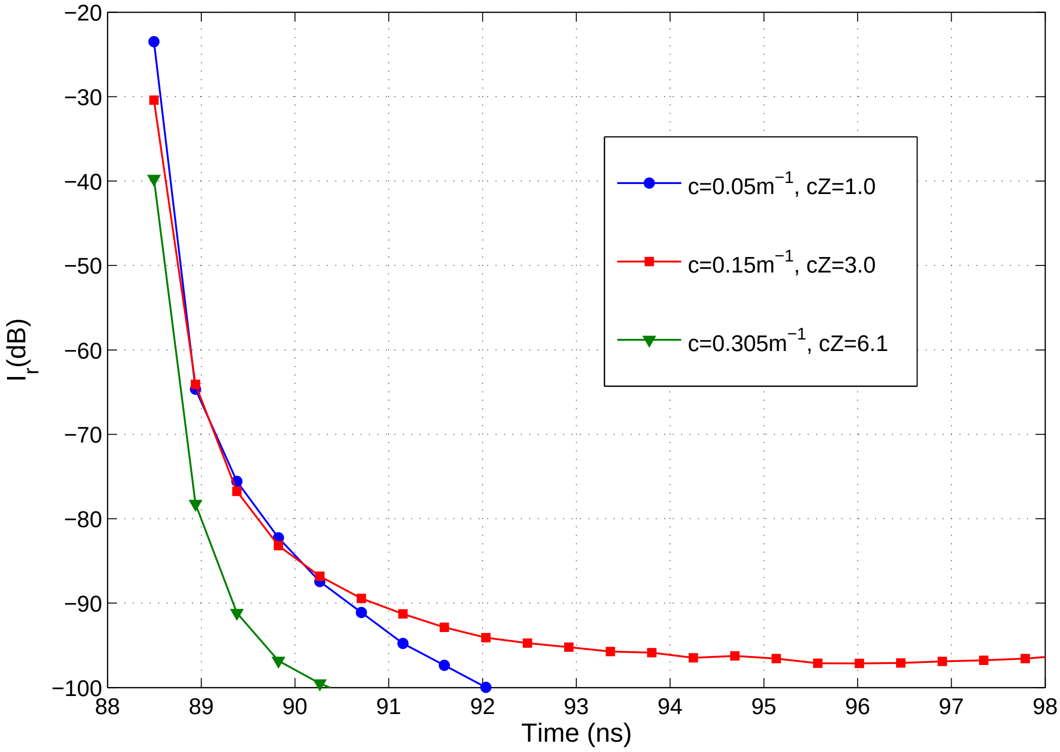

Fig. 5. CIR (received intensity as a function of time) for pure sea, clean ocean, and coastal waters. $Z = 20\,\mathrm{m}$ and $D = 20\,\mathrm{cm}$.

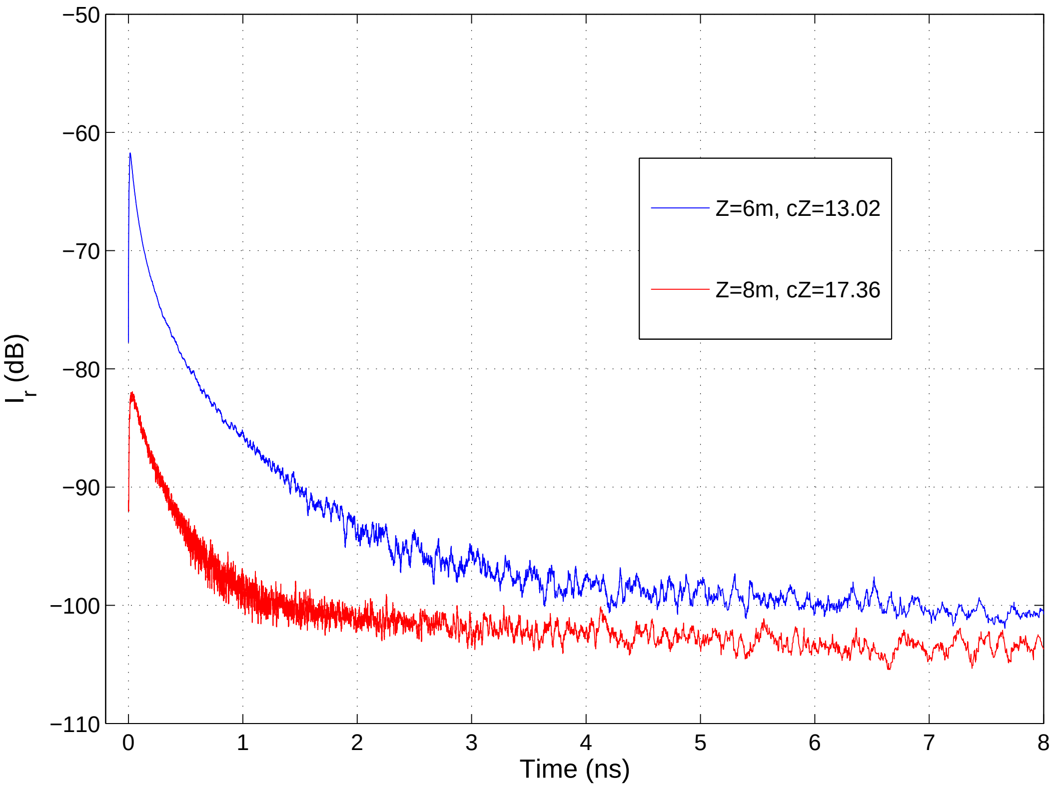

Fig. 6. CIR for turbid harbor waters with $c = 2.17\,\mathrm{m}^{-1}$. $\theta = 20^{\circ}$, and $D = 20\,\mathrm{cm}$. The abscissa is with reference to the absolute propagation time from the transmitter to the receiver.

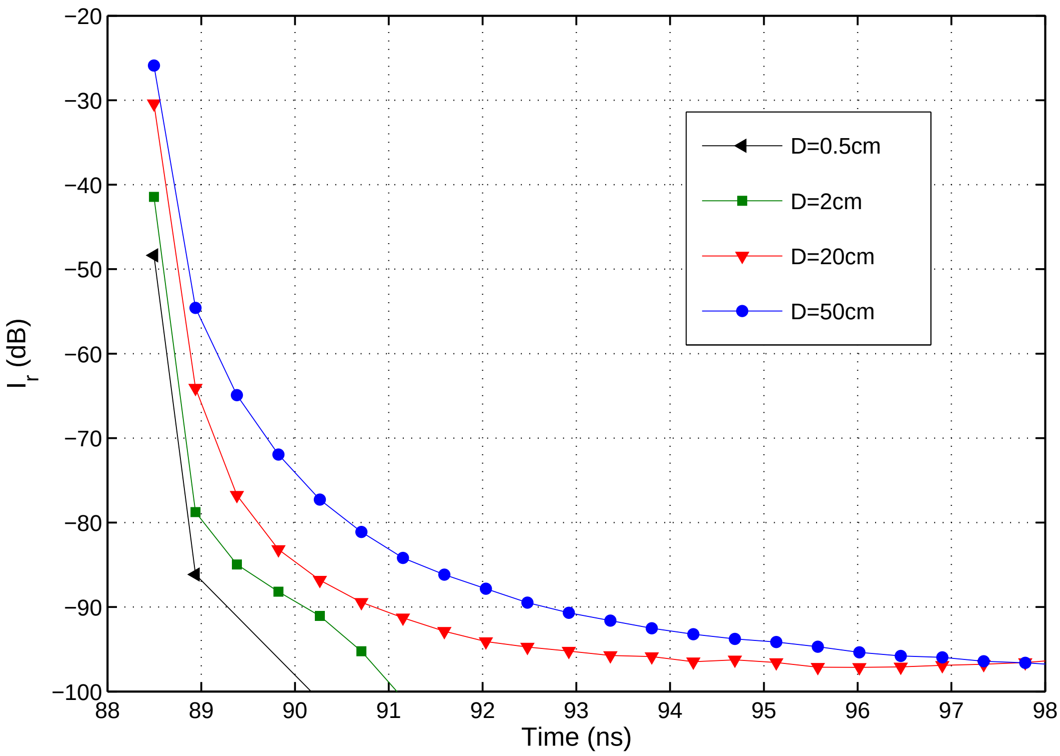

Fig. 7. CIR for different receiver aperature diameters D. $Z = 20\,\mathrm{m}$, clear ocean waters, $cZ = 3.0$.

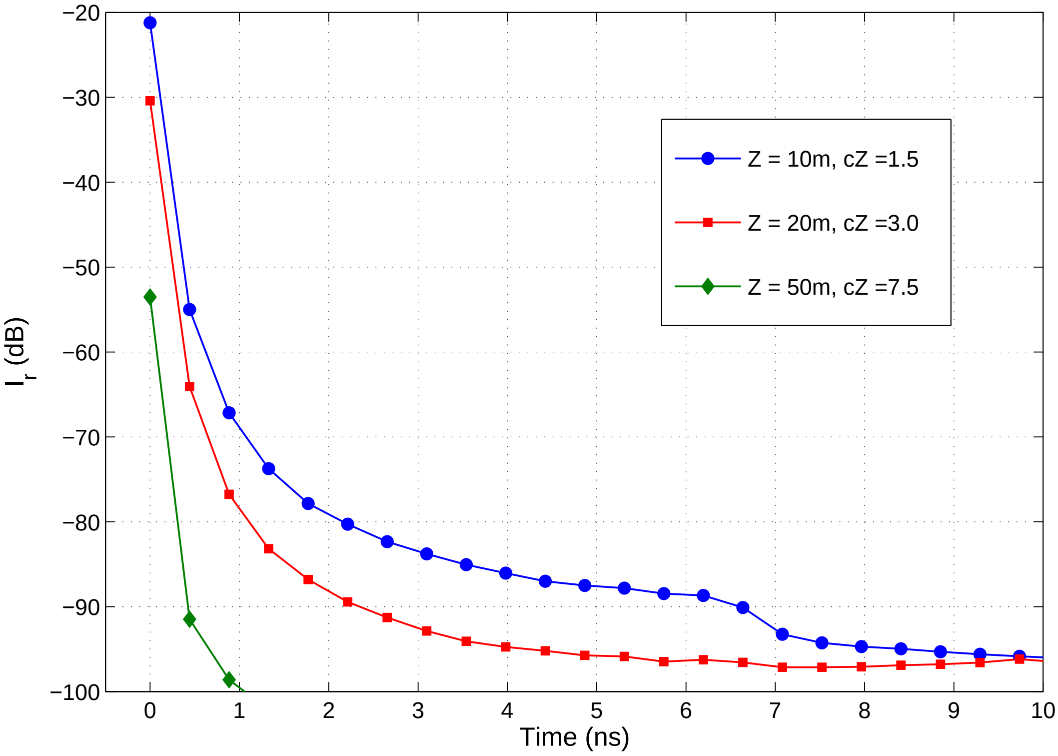

Fig. 8. Shifted CIR for different link distances Z. $D = 20\,\text{cm}$, clear ocean waters. The abscissa is with reference to the absolute propagation time from the transmitter to the receiver.

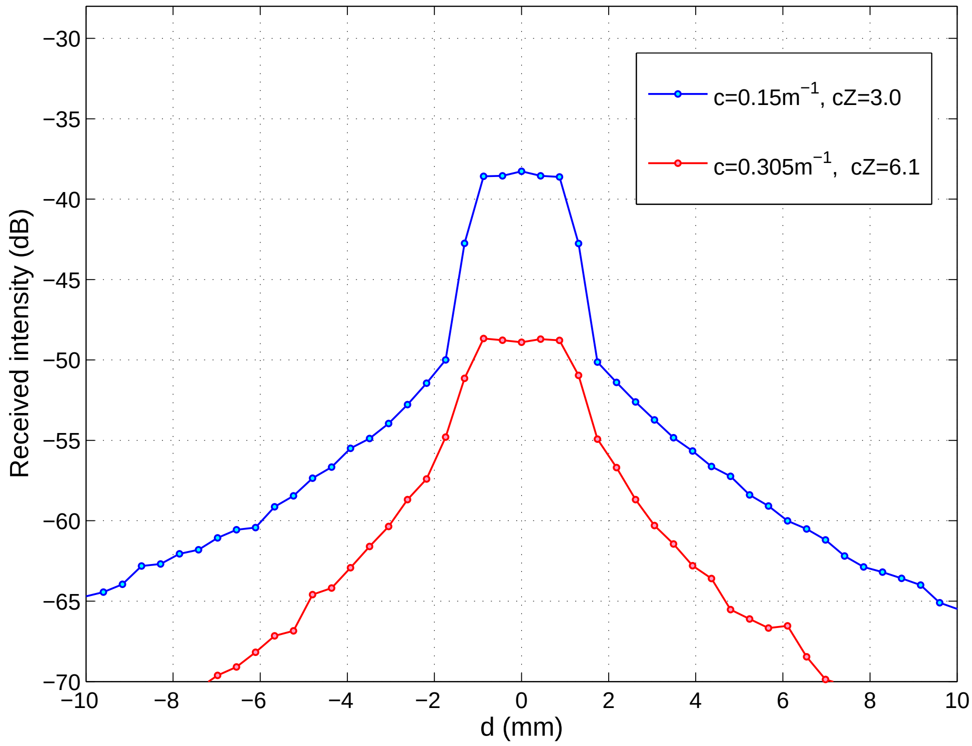

Fig. 9. Received photon distribution on the receiver lens focal plane. Clean ocean waters, $D = 20\,\text{cm}$, $F = 25\,\text{cm}$.

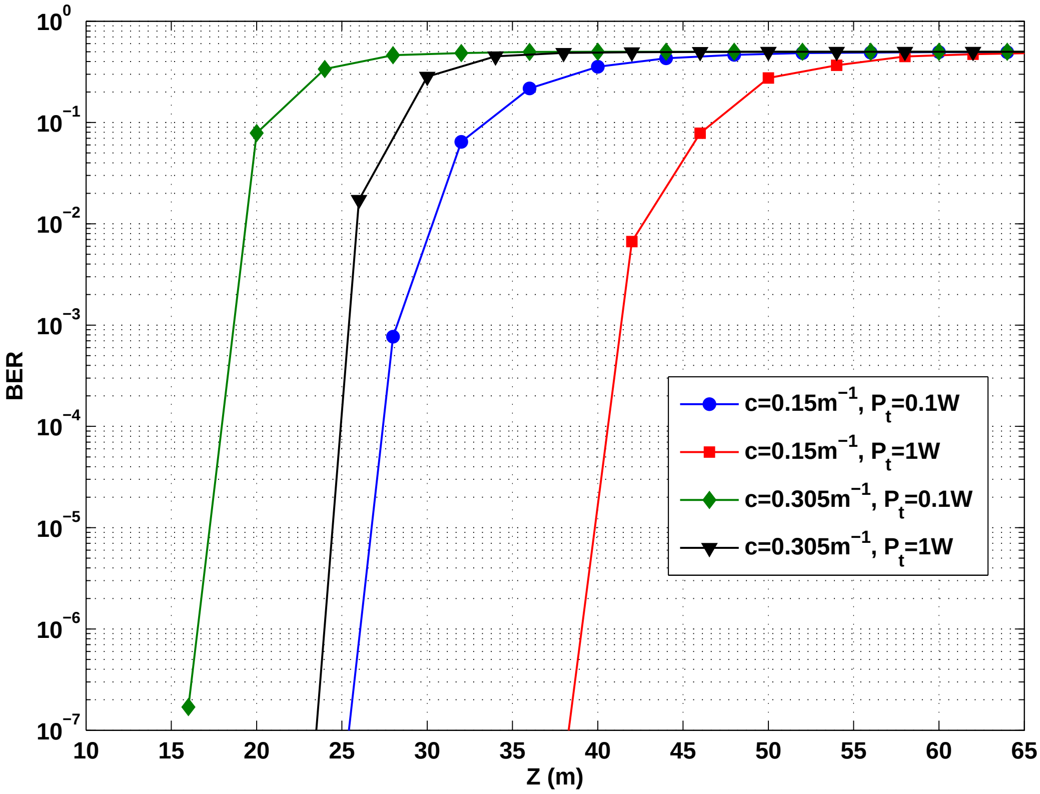

Fig. 10. BER performance as a function of distance Z for different transmit optical powers P_t for the case of PIN PD. Clear ocean and coastal waters, $D = 20\,\text{cm}$.

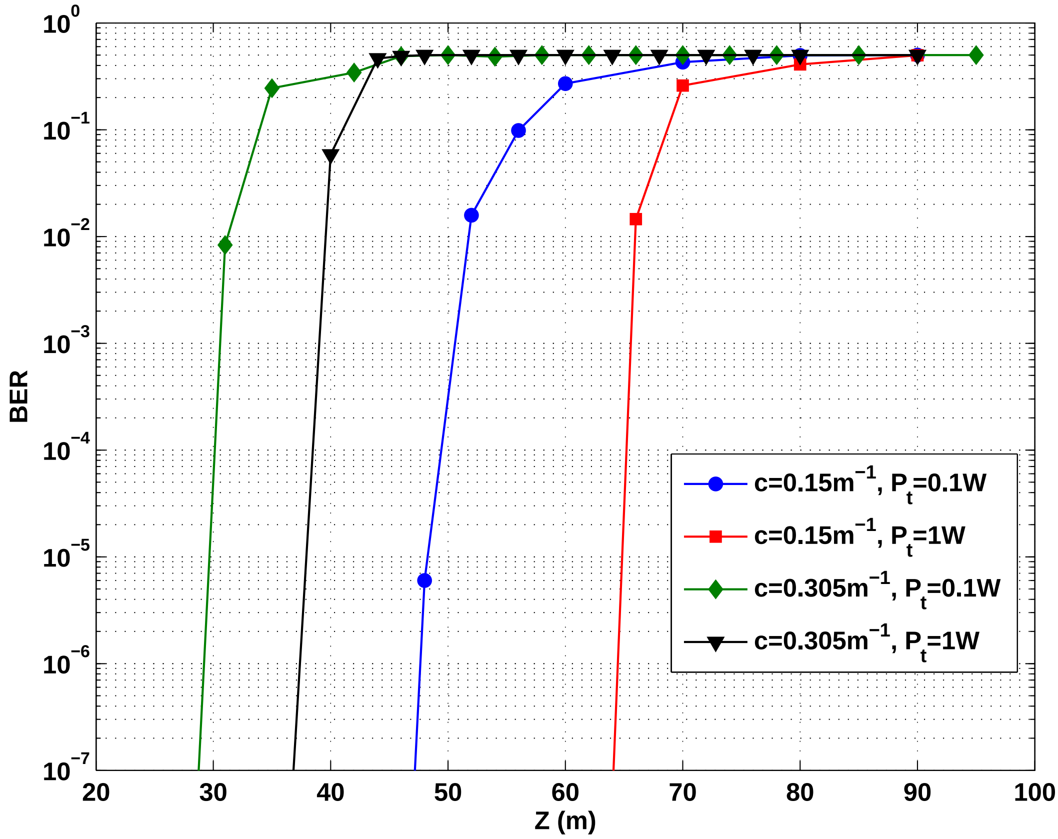

Fig. 11. BER performance as a function of distance Z for different transmit optical powers P_t for the case of APD. Clear ocean and coastal waters, $D = 20\,\mathrm{cm}$.